

Abstract

In order to optimize surface CO₂ fluxes at finer scales, a regional surface CO₂ flux inversion system (Carbon Flux Inversion system and Community Multi-scale Air Quality, CFI-CMAQ) has been developed by simultaneously assimilating CO₂ concentrations and surface CO₂ fluxes into the regional modeling system, CMAQ. The smoothing operator is associated with the atmospheric transport model to constitute a persistence dynamical model to forecast the surface CO₂ flux scaling factors. In this implementation, the “signal-to-noise” problem can be avoided; plus, any useful observed information achieved by the current assimilation cycle can be transferred into the next assimilation cycle. Thus, the surface CO₂ fluxes can be optimized as a whole at the grid scale in CFI-CMAQ. The performance of CFI-CMAQ was quantitatively evaluated through a set of Observing System Simulation Experiments (OSSEs) by assimilating CO₂ retrievals from GOSAT (Greenhouse Gases Observing Satellite). The results showed that the CO₂ concentration assimilation using the ensemble Kalman filter (EnKF) could constrain the CO₂ concentrations effectively, illustrating that the simultaneous assimilation of CO₂ concentrations can provide convincing CO₂ initial analysis fields for CO₂ flux inversion. In addition, the CO₂ flux optimization using the ensemble Kalman smoother (EnKS) demonstrated that CFI-CMAQ could in general reproduce true fluxes at finer scales with acceptable bias. Two further sets of numerical experiments were conducted to investigate the sensitivities of the inflation factor of scaling factors and the smoother window. The results showed that the ability of CFI-CMAQ to optimize CO₂ fluxes greatly relied on the choice of the inflation factor. However, the smoother window had a slight influence on the optimized results. CFI-CMAQ performed very well even with a short lag-window (e.g. 3 days).

A regional carbon flux data assimilation system

Z. Peng et al.

Title Page

Abstract

Introduction

Conclusions

References

Tables

Figures



Back

Close

Full Screen / Esc

Printer-friendly Version

Interactive Discussion



1 Introduction

Atmospheric CO₂ concentrations are increasing due to fossil fuel combustion, cement production, and land use changes such as deforestation. As the most important anthropogenic greenhouse gas, the accumulation of CO₂ in the atmosphere is reported to be the largest human-induced driver of global warming (IPCC AR5 WG1: 2013), providing a substantial threat to the sustainable development of both the environment and mankind. Quantifying CO₂ sources and sinks is central to the successful implementation of carbon emissions reduction strategies aimed at mitigating the adverse effects of global warming. It is possible to improve the accuracy of surface CO₂ flux estimates through the use of an advanced data assimilation technique (e.g., Chevallier et al., 2005, 2007; Chevallier, 2007; Baker et al., 2006; Peters et al., 2007; Engelen et al., 2009; Feng et al., 2009; Kang et al., 2012; Liu et al., 2012). Feng et al. (2009) showed that the uncertainties of surface CO₂ flux estimates can be reduced significantly by assimilating OCO X_{CO₂} measurements. Peters et al. (2005, 2007, 2009) developed a surface CO₂ flux inversion system, CarbonTracker, by incorporating the ensemble square-root filter (EnSRF) into the atmospheric transport TM5 model. And the inversion results obtained by assimilating in situ surface CO₂ observations are in excellent agreement with a wide collection of carbon inventories that form the basis of the first North American State of the Carbon Cycle Report (SOCCR) (Peters et al., 2007). CarbonTracker is also well used to constrain the surface CO₂ flux over Europe and Asia (eg., Zhang et al., 2014a, b). Kang et al. (2011, 2012) presented a simultaneous data assimilation of surface CO₂ fluxes and atmospheric CO₂ concentrations along with meteorological variables using the Local Ensemble Transform Kalman Filter (LETKF). They indicated that an accurate estimation of the evolving surface fluxes can be gained even without any a priori information. Recently, Tian et al. (2013) developed a new surface CO₂ flux data assimilation system, Tan-Tracker (in Chinese, “Tan” means carbon), by incorporating a joint PODEn4DVar assimilation framework into the GEOS-Chem model on the basis of Peters et al. (2005, 2007) and Kang et al. (2011, 2012).

**A regional carbon
flux data assimilation
system**

Z. Peng et al.

[Title Page](#)[Abstract](#)[Introduction](#)[Conclusions](#)[References](#)[Tables](#)[Figures](#)[Back](#)[Close](#)[Full Screen / Esc](#)[Printer-friendly Version](#)[Interactive Discussion](#)

They discussed in detail that the assimilation of CO₂ surface fluxes could be improved though the use of simultaneous assimilation of CO₂ concentrations and CO₂ surface fluxes due to the fact that the uncertainty of the evolution of CO₂ concentrations could be gradually eliminated. Despite the rigor of data assimilation theory, current CO₂ flux-inversion methods (e.g., CarbonTracker) still face many challenging scientific problems, such as: (1) the well-known “signal-to-noise” problem (NRC, 2010); (2) large inaccuracies in chemical transport models (e.g., Prather et al., 2008); (3) vast computational expenses (e.g., Feng et al., 2009); and (4) the sparseness of observation data (e.g., Gurney et al., 2002).

The “signal-to-noise” problem is one of the most challenging issue for an ensemble-based CO₂ flux inversion system due to the fact that surface CO₂ fluxes are the model forcing (or boundary condition), rather than model states (like CO₂ concentrations), of the chemistry transport model (CTM). In the absence of a suitable dynamical model to describe the evolution of the surface CO₂ fluxes, most CO₂ flux-inversion studies have traditionally ignored the uncertainty of anthropogenic and other CO₂ emissions and focused on the optimization of natural (i.e., biospheric and oceanic) CO₂ emissions at the ecological scale (e.g., Deng et al., 2007; Feng et al., 2009; Peters et al., 2005, 2007; Jiang et al., 2013; Peylin et al., 2013).

This compromise is acceptable to some extent. Indeed, the total amount of anthropogenic CO₂ emissions can be estimated by relatively well-documented global fuel-consumption data with a small degree of uncertainty (Boden et al., 2011). It was reported in IPCC (2007) that anthropogenic CO₂ emissions were the primary source contributing to the $7.2 \pm 0.3 \text{ Pg C yr}^{-1}$ from 2000 to 2005; ocean–atmosphere exchanges were the largest sinks, absorbing $-2.2 \pm 0.5 \text{ Pg C yr}^{-1}$, followed by biosphere–atmosphere exchanges, absorbing $-0.9 \pm 0.6 \text{ Pg C yr}^{-1}$ during the same period. There is no doubt that the uncertainties involved in the total amount of anthropogenic CO₂ emissions are much smaller than those related to natural emissions.

However, their spatial distribution, strength and temporal development still remain elusive, because of their inherent non-uniformities (Andres et al., 2012; Gurney et al.,

A regional carbon flux data assimilation system

Z. Peng et al.

Title Page

Abstract

Introduction

Conclusions

References

Tables

Figures



Back

Close

Full Screen / Esc

Printer-friendly Version

Interactive Discussion



2009). With increasing scientific and political interest in recent years, information on anthropogenic CO₂ emissions is required at increasingly finer scales, in addition to quantifying their total amount. Marland (2008) pointed out that even a tiny amount of uncertainty, i.e., 0.9%, in one of the leading emitter countries like the US is equivalent to the total emissions of the smaller emitter countries in the world. Furthermore, the usual values of anthropogenic CO₂ emissions in chemical transport models have thus far been simply interpolated from very coarse monthly-mean fuel consumption data. Therefore, great uncertainty in the spatiotemporal distributions of anthropogenic emissions likely exists, which could reduce the accuracy of CO₂ concentration simulations and subsequently increase the inaccuracy of natural CO₂ flux inversion results. In addition, current research approaches tend only to assimilate natural CO₂ emissions at the ecological scale, which is far from sufficient. Therefore, surface CO₂ fluxes should be constrained as a whole at a finer scale.

In CarbonTracker (Peters et al., 2007), a smoothing operator is innovatively applied as the persistence forecast model. In that application, the surface CO₂ fluxes can be treated as the model states and the observed information ingested by the current assimilation cycle can be used in the next assimilation cycle effectively. However, the “signal-to-noise” problem is not yet resolved, and thus CarbonTracker also has to assimilate natural CO₂ emissions at the ecological scale only. In Tan-Tracker (Tian et al., 2013), a 4-D moving sampling strategy (Wang et al., 2010) is used to generate the flux ensemble members, and so the surface CO₂ fluxes can be optimized as a whole at the grid scale. In the present reported work, the persistence dynamical model taken by Peters et al. (2005) was further developed for the purpose of resolving the “signal-to-noise” problem, as well as transporting the useful observed information in the next assimilation cycle, in order to optimize the surface CO₂ fluxes as a whole at the grid scale. This process is described in detail in Sect. 2 of this paper.

The surface CO₂ flux inversion system presented in this paper was developed by incorporating a joint data assimilation framework into a regional modeling system to optimize the CO₂ fluxes at a finer scale. A joint assimilation framework – the simultane-

**A regional carbon
flux data assimilation
system**

Z. Peng et al.

Title Page

Abstract

Introduction

Conclusions

References

Tables

Figures



Back

Close

Full Screen / Esc

Printer-friendly Version

Interactive Discussion



ous assimilation of CO₂ concentrations and surface CO₂ fluxes – was applied because assimilating CO₂ observations from multiple sources can improve the accuracy of simulation results (e.g., Miyazaki, 2009; Liu et al., 2009, 2011, 2012; Tangborn et al., 2013; Huang et al., 2014), and the simultaneous assimilation of CO₂ concentrations and surface CO₂ fluxes can largely eliminate the uncertainty in initial CO₂ concentrations on the CO₂ evolution (Kang et al., 2011, 2012; Tian et al., 2013). The data assimilation techniques applied were the ensemble Kalman filter (EnKF) and the ensemble Kalman smoother (EnKS). EnKF was used to constrain CO₂ concentrations and EnKS was used to optimize surface CO₂ fluxes. The regional transport modeling system applied was Regional Atmospheric Modeling System and Community Multi-scale Air Quality (RAMS-CMAQ). Previous studies (Ahmadov et al., 2009; Pillai et al., 2010; Kretschmer et al., 2011) have shown that regional chemical transport models with high resolution, compared to global models, can reduce model errors and may have the ability to reproduce the effects of meso–micro–scale transport on atmospheric CO₂ distributions. Besides, RAMS-CMAQ has been proven to be reliable (Zhang et al., 2002, 2003, 2007; Kou et al., 2013; Liu et al., 2013; Huang et al., 2014). Thus, RAMS-CMAQ was chosen to develop this regional surface CO₂ flux inversion system. For simplicity, this system is referred to as CFI-CMAQ (Carbon Flux Inversion system and Community Multi-scale Air Quality).

Since this is the first time of introducing CFI-CMAQ, we focus mainly on introducing the methodology in this paper. Nevertheless, in addition, Observing System Simulation Experiments (OSSEs) were designed to assess the system's ability to optimize surface CO₂ fluxes. The information of GOSAT X_{CO} are used to generate artificial observations because of the sparseness and heterogeneity of ground-based measurements.

The remainder of the paper is organized as follows. Section 2 describes the details of the regional surface CO₂ flux inversion system, CFI-CMAQ, including the developed persistence dynamical model, a simple review of the EnKS and EnKF assimilation approaches, and the process involved. The experimental designs are then introduced

and the assimilation results shown in Sect. 3. Finally, a summary and conclusions are provided in Sect. 4.

2 Framework of the regional surface CO₂ flux inversion system

As an ensemble-based assimilation system, CFI-CMAQ was also developed by applying a set of linear multiplication factors, similar to the approach by Peters et al. (2007) and Tian et al. (2013). Therefore, the background surface fluxes from an N -member ensemble can be described by

$$F_i^b(x, y, z, t) = \lambda_i^b(x, y, z, t) F^0(x, y, z, t), \quad (i = 1, \dots, N), \quad (1)$$

where $F_i^b(x, y, z, t)$ are the background fluxes that force the CTM to integrate to produce the background CO₂ concentration fields, $F^0(x, y, z, t)$ are the prior net CO₂ surface exchanges, and $\lambda_i^b(x, y, z, t)$ represent the background linear scaling factors (Peters et al., 2007; Tian et al., 2013) for each time and each grid to be optimized in the assimilation. The notation is standard: the superscript b refers to the background, and the subscript i refers to the i th ensemble member. In the following, $\lambda_i^b(x, y, z, t)$ are referred to as $\lambda_{i,t}^b$ for simplicity.

At each optimization cycle, CFI-CMAQ includes the following four parts: (1) forecasting of the background linear scaling factors $\lambda_{i,t}^b$; (2) optimization of the scaling factors in the smoother window by EnKS (see Fig. 1); (3) updating of the flux in the smoother window; and (4) assimilation of the CO₂ concentration fields at time t by EnKF. A flowchart illustrating CFI-CMAQ is presented in Fig. 2. The assimilation procedure is addressed in detail below. In addition, the observation operator is introduced, particularly for use of the GOSAT X_{CO_2} data in Sect. 2.5. Furthermore, covariance inflation and localization techniques applied in CFI-CMAQ are introduced briefly in Sect. 2.6.

A regional carbon flux data assimilation system

Z. Peng et al.

Title Page

Abstract

Introduction

Conclusions

References

Tables

Figures



Back

Close

Full Screen / Esc

Printer-friendly Version

Interactive Discussion



2.1 Forecasting the background linear scaling factors

In order to pass the useful observed information onto the next assimilation cycle effectively, following Peters et al. (2007) the smoothing operator is applied as the persistence dynamical model to calculate the linear scaling factors $\lambda_{i,t}^b$,

$$\lambda_{i,t}^b = \frac{\left(\sum_{j=t-M+1}^{t-1} \lambda_{i,j|t-1}^a + \lambda_{i,t}^p \right)}{M}, \quad (j = 1, \dots, N, j = t - M + 1, \dots, t - 1), \quad (2)$$

where $\lambda_{i,j|t-1}^a$ refers to analyzed quantities from the previous assimilation cycle at time j (see Fig. 1) and $|t-1$ means that these factors have been optimized by using observations at time $t-1$; $\lambda_{i,t}^p$ refers to the prior values of the linear scaling factors at time t . The superscript a refers to the analyzed, and p refers to the prior. This operation represents a smoothing over all the time steps in the smoother window (see Fig. 1), thus dampening variations in the forecast of $\lambda_{i,t}^b$ in time.

In order to generate $\lambda_{i,t}^b$, the atmospheric transport model (CMAQ) is applied and a set of ensemble forecast experiments are carried out to obtain the prior values for $\lambda_{i,t}^p$. It integrates from time $t-1$ to t to produce the CO₂ concentration fields $C_i^f(x, y, z, t)$ forced by the prior flux $F_0(x, y, z, t)$ with $C_i^a(x, y, z, t-1)$ as initial conditions. Then, the ratio $\kappa_{i,t} = \frac{C_i^f(x, y, z, t)}{C_i^a(x, y, z, t)}$ is calculated, where $C_i^f(x, y, z, t) = \frac{1}{N} \sum_{i=1}^N C_i^f(x, y, z, t)$. Suppose that $\lambda_{i,t}^p = \kappa_{i,t}$ due to the fact that the surface CO₂ fluxes correlate with its concentrations, the values for $\lambda_{i,t}^p$ are obtained and then $\lambda_{i,t}^b$ can finally be calculated (see the part with red arrows in the flowchart in Fig. 2). Hereafter, $C_i^f(x, y, z, t)$ are referred to as $C_{i,t}^f$ for simplicity.

The assumption $\lambda_{i,t}^p = \kappa_{i,t}$ is just a compromise from the complex conservation equation. In CarbonTracker, $\lambda_{i,t}^p$ are all set to 1 (Peters et al., 2007). In this study, the smooth-

Title Page

Abstract

Introduction

Conclusions

References

Tables

Figures



Back

Close

Full Screen / Esc

Printer-friendly Version

Interactive Discussion



A regional carbon flux data assimilation system

Z. Peng et al.

Title Page

Abstract

Introduction

Conclusions

References

Tables

Figures

◀

▶

◀

▶

Back

Close

Full Screen / Esc

Printer-friendly Version

Interactive Discussion



ing operator is associated with the atmospheric transport model to constitute the persistence dynamical model to describe the evolution of the scaling factors. Through this process, the prior values of $\lambda_{i,t}^p$ can be forecast at the grid scale without any random noise. So do $\lambda_{i,t}^b$. Ultimately, the “signal-to-noise” problem can be resolved, and the surface CO₂ fluxes can then be optimized as a whole at the grid scale.

It is important to note that, similar to Peters et al. (2007), this dynamical model equation still does not include an error term in the dynamical model, and the model error cannot yet be estimated. However, the covariance inflation is applied to compensate for model errors before optimization, which is addressed in Sect. 2.6.

2.2 Optimizing the scaling factors in the smoother window by EnKS

In the current assimilation cycle $t - M \sim t$ (see Fig. 1), the scaling factors to be optimized in the smoother window are $(\lambda_{i,t-M|t-1}^a, \lambda_{i,t-M+1|t-1}^a, \dots, \lambda_{i,j|t-1}^a, \dots, \lambda_{i,t-1|t-1}^a, \lambda_{i,t}^b)$. Referring to $\lambda_{i,t}^b$ as $\lambda_{i,t|t-1}^a$ for convenience, the scaling factors to be optimized are $(\lambda_{i,t-M|t-1}^a, \lambda_{i,t-M+1|t-1}^a, \dots, \lambda_{i,j|t-1}^a, \dots, \lambda_{i,t-1|t-1}^a, \lambda_{i,t|t-1}^a)$. Using the EnKS analysis technique, these scaling factors are updated in turn via

$$\lambda_{i,j|t}^a = \lambda_{i,j|t-1}^a + \mathbf{K}^e \left(\mathbf{y}_t^{\text{obs}} - \mathbf{y}_{i,t}^f + \nu_{i,t} \right), \quad (i = 1, \dots, N, j = t - M + 1, \dots, t - 1), \quad (3)$$

$$\mathbf{K}^e = \mathbf{S}_{j,t|t-1}^e \mathbf{H}^T (\mathbf{H} \mathbf{P}_{t,t|t-1}^e \mathbf{H}^T + \mathbf{R})^{-1}, \quad (4)$$

$$\mathbf{S}_{j,t|t-1}^e = \frac{1}{N-1} \sum_{i=1}^N \left[\lambda_{i,j|t-1}^a - \overline{\lambda_{i,j|t-1}^a} \right] \left[\lambda_{i,t|t-1}^a - \overline{\lambda_{i,t|t-1}^a} \right]^T, \quad (5)$$

$$\mathbf{P}_{t,t|t-1}^e = \frac{1}{N-1} \sum_{i=1}^N \left[\lambda_{i,t|t-1}^a - \overline{\lambda_{i,t|t-1}^a} \right] \left[\lambda_{i,t|t-1}^a - \overline{\lambda_{i,t|t-1}^a} \right]^T, \quad (6)$$

$$\mathbf{y}_{i,t}^f = \mathbf{H} \left(\mathbf{M}_{t-1 \rightarrow t} \left(\lambda_{i,t|t-1}^a \right) \right), \quad (7)$$

A regional carbon flux data assimilation system

Z. Peng et al.

Title Page	
Abstract	Introduction
Conclusions	References
Tables	Figures
◀	▶
◀	▶
Back	Close
Full Screen / Esc	
Printer-friendly Version	
Interactive Discussion	

where \mathbf{K}^e is the Kalman gain matrix of EnKS, $\mathbf{S}_{j,t|t-1}^e$ is the background error cross-covariance between the state vector $\lambda_{i,j|t-1}^a$ and $\lambda_{i,t|t-1}^a$, $\mathbf{P}_{t,t|t-1}^e$ is the background error covariance of the state vector $\lambda_{i,t|t-1}^a$, $H(\cdot)$ is the observation operator that maps the state variable from model space into observation space, $v_{i,t}$ is a random normal distribution perturbation field with zero mean and \mathbf{R} standard deviation representing the measurement errors, $\mathbf{y}_t^{\text{obs}}$ is the observation vector measured at time t and $\mathbf{y}_{i,t}^f$ is the simulated observations.

In actual implementations, it is unnecessary to calculate $\mathbf{S}_{j,t|t-1}^e$ and $\mathbf{P}_{t,t|t-1}^e$ separately. $\mathbf{S}_{j,t|t-1}^e H^T$ and $H \mathbf{P}_{t,t|t-1}^e H^T$ can be calculated as a whole by

$$\mathbf{S}_{j,t|t-1}^e H^T = \frac{1}{N-1} \sum_{i=1}^N \left[\lambda_{i,j|t-1}^a - \overline{\lambda_{i,j|t-1}^a} \right] \left[\mathbf{y}_{i,t}^f - \overline{\mathbf{y}_t^f} \right]^T, \tag{8}$$

$$H \mathbf{P}_{t,t|t-1}^e H^T = \frac{1}{N-1} \sum_{i=1}^N \left[\mathbf{y}_{i,t}^f - \overline{\mathbf{y}_t^f} \right] \left[\mathbf{y}_{i,t}^f - \overline{\mathbf{y}_t^f} \right]^T, \tag{9}$$

$$\overline{\mathbf{y}_t^f} = \frac{1}{N-1} \sum_{i=1}^N \mathbf{y}_{i,t}^f. \tag{10}$$

2.3 Updating the flux in the smoother window

Substituting the optimized scaling factors $(\lambda_{i,t-M|t}^a, \lambda_{i,t-M+1|t}^a, \dots, \lambda_{i,j|t}^a, \dots, \lambda_{i,t-1|t}^a, \lambda_{i,t|t}^a)$ into Eq. (1), the flux in the smoother window can be updated.



2.4 Assimilating the CO₂ concentration fields at time t by EnKF

The analysis of CO₂ concentrations fields at time t in the EnKF scheme is updated via

$$\mathbf{C}_{i,t}^a = \mathbf{C}_{i,t}^f + K \left(\mathbf{y}_t^{\text{obs}} - \mathbf{y}_t^f + \nu_{i,t} \right), \quad (11)$$

$$K = \mathbf{P}^f H^T \left(H \mathbf{P}^f H^T + \mathbf{R} \right)^{-1}, \quad (12)$$

where K is the Kalman gain matrix of EnKF and \mathbf{P}^f is the background error covariance among the forecasted CO₂ concentration fields $\mathbf{C}_{i,t}^f$. $\mathbf{P}^f H^T$ and $H \mathbf{P}^f H^T$ can be calculated as a whole by

$$\mathbf{P}^f H^T = \frac{1}{N-1} \sum_{i=1}^N \left[\mathbf{C}_{i,t}^f - \overline{\mathbf{C}_{i,t}^f} \right] \left[\mathbf{y}_{i,t}^f - \overline{\mathbf{y}_t^f} \right]^T, \quad (13)$$

$$H \mathbf{P}^f H^T = \frac{1}{N-1} \sum_{i=1}^N \left[\mathbf{y}_{i,t}^f - \overline{\mathbf{y}_t^f} \right]^T \left[\mathbf{y}_{i,t}^f - \overline{\mathbf{y}_t^f} \right]. \quad (14)$$

2.5 The observation operator

As mentioned above, the observation operator $H(\cdot)$ transforms the state variable from model space into observation space. Usually, it is the spatial bilinear interpolator for traditional ground-based observations. Since the GOSAT X_{CO_2} retrieval is a weighted CO₂ column average, the simulated X_{CO_2} should be calculated with the same weighted column average method (Connor et al., 2008; Crisp et al., 2010, 2012; O'Dell et al., 2012). So, the observation operator to assimilate the GOSAT X_{CO_2} retrieval is

$$\mathbf{y}^f = H \left(M_{t-1 \rightarrow t} \left(\boldsymbol{\lambda}_{i,t|t-1}^a \right) \right) = H \left(\mathbf{C}_{i,t}^f \right) = \mathbf{y}^{\text{priori}} + h^T \mathbf{a}_{\text{CO}_2} \left(S \left(\mathbf{C}_{i,t}^f \right) - \mathbf{r}^{\text{priori}} \right), \quad (15)$$

where \mathbf{y}^f is the simulated X_{CO_2} ; $\mathbf{y}^{\text{priori}}$ is the a priori CO₂ column average used in the GOSAT X_{CO_2} retrieval process; $S(\cdot)$ is the spatial bilinear interpolation operator that

Title Page

Abstract

Introduction

Conclusions

References

Tables

Figures



Back

Close

Full Screen / Esc

Printer-friendly Version

Interactive Discussion



interpolates the simulated fields to the GOSAT X_{CO_2} locations to obtain the simulated CO_2 vertical profiles there; $\mathbf{r}^{\text{priori}}$ is the a priori CO_2 vertical profile used in the retrieval process; h is the pressure weighting function, which indicates the contribution of the retrieved value from each layer of the atmosphere; and \mathbf{a}_{CO_2} is the normalized averaging kernel.

2.6 Covariance inflation and localization

In order to keep the ensemble spread of the CO_2 concentrations at a certain level and compensate for transport model error to prevent filter divergence, covariance inflation is applied before updating the CO_2 concentrations. So,

$$(\mathbf{C}_{i,t}^f)_{\text{new}} = \alpha \left(\mathbf{C}_{i,t}^f - \overline{\mathbf{C}_{i,t}^f} \right) + \overline{\mathbf{C}_{i,t}^f}, \quad (16)$$

where α is the inflation factor of CO_2 concentrations and $(\mathbf{C}_{i,t}^f)_{\text{new}}$ is the final field used for data assimilation.

Similarly, covariance inflation is also used to keep the ensemble spread of the prior scaling factors at a certain level and compensate for dynamical model error. So,

$$(\boldsymbol{\lambda}_{i,t}^p)_{\text{new}} = \beta \left(\boldsymbol{\lambda}_{i,t}^p - \overline{\boldsymbol{\lambda}_{i,t}^p} \right) + \overline{\boldsymbol{\lambda}_{i,t}^p}, \quad (17)$$

where β is the inflation factor of scaling factors and $(\boldsymbol{\lambda}_{i,t}^p)_{\text{new}}$ is the final scaling factors used for data assimilation.

In addition, the Schur product is utilized to filter the remote correlation resulting from the spurious long-range correlations (Houtekamer and Mitchell, 2001). So, the Kalman

A regional carbon flux data assimilation system

Z. Peng et al.

Title Page

Abstract

Introduction

Conclusions

References

Tables

Figures



Back

Close

Full Screen / Esc

Printer-friendly Version

Interactive Discussion



gain matrix \mathbf{K}^e and K are updated via

$$\mathbf{K}^e = \left[\left(\boldsymbol{\rho} \circ \mathbf{S}_{j,t|t-1}^e \right) H^T \left(H \left(\boldsymbol{\rho} \circ \mathbf{P}_{t,t|t-1}^e \right) H^T + \mathbf{R} \right)^{-1} \right], \quad (18)$$

$$K = \left[\left(\boldsymbol{\rho} \circ \mathbf{P}^f \right) H^T \right] \left[\left(H \left(\boldsymbol{\rho} \circ \mathbf{P}^f \right) H^T + \mathbf{R} \right)^{-1} \right], \quad (19)$$

5 where the filtering matrix $\boldsymbol{\rho}$ is calculated using the formula

$$C_0(r, c) = \begin{cases} -\frac{1}{4} \left(\frac{|r|}{c} \right)^5 + \frac{1}{2} \left(\frac{|r|}{c} \right)^4 + \frac{5}{8} \left(\frac{|r|}{c} \right)^3 - \frac{5}{3} \left(\frac{|r|}{c} \right)^2 + 1, & 0 \leq |r| \leq c \\ \frac{1}{12} \left(\frac{|r|}{c} \right)^5 - \frac{1}{2} \left(\frac{|r|}{c} \right)^4 + \frac{5}{8} \left(\frac{|r|}{c} \right)^3 + \\ \frac{5}{3} \left(\frac{|r|}{c} \right)^2 - 5 \left(\frac{|r|}{c} \right) + 4 - \frac{2}{3} \left(\frac{c}{|r|} \right), & c \leq |r| \leq 2c \\ 0, & c \leq |r| \end{cases}, \quad (20)$$

10 where c is the element of the localization Schur radius. The matrix $\boldsymbol{\rho}$ can filter the small background error correlations associated with remote observations through the Schur product (Tian et al., 2011). And the Schur product tends to reduce the effect of those observations smoothly at intermediate distances due to the smooth and monotonically decreasing of the filtering matrix.

3 OSSEs for evaluation of CFI-CMAQ

A set of OSSEs were designed to quantitatively assess the performance of CFI-CMAQ. The setup of the experiments and the results are described in this section.

3.1 Experimental setup

The chemical transport model utilized was RAMS-CMAQ (Zhang et al., 2002), in which CO_2 was treated as an inert tracer. The model domain was 6654 km \times 5440 km on a ro-

Title Page

Abstract

Introduction

Conclusions

References

Tables

Figures

⏪

⏩

◀

▶

Back

Close

Full Screen / Esc

Printer-friendly Version

Interactive Discussion



A regional carbon flux data assimilation system

Z. Peng et al.

Title Page

Abstract

Introduction

Conclusions

References

Tables

Figures



Back

Close

Full Screen / Esc

Printer-friendly Version

Interactive Discussion



tated polar stereographic map projection centered at (35.0° N, 116.0° E), with a horizontal grid resolution of 64 km × 64 km and 15 vertical layers in the σ_2 -coordinate system, unequally spaced from the surface to approximately 23 km. The initial fields and boundary conditions of the CO₂ concentrations were interpolated from the simulated CO₂ fields of CarbonTracker 2011 (Peters, 2007). The prior surface CO₂ fluxes included biosphere–atmosphere CO₂ fluxes, ocean–atmosphere CO₂ fluxes, anthropogenic emissions, and biomass-burning emissions (Kou et al., 2013),

$$F^0(x, y, z, t) = F_{\text{bio}}(x, y, z, t) + F_{\text{oce}}(x, y, z, t) + F_{\text{ff}}(x, y, z, t) + F_{\text{fire}}(x, y, z, t), \quad (21)$$

where $F^0(x, y, z, t)$ was the prior surface CO₂ flux; F_{bio} and F_{oce} were the biosphere–atmosphere and ocean–atmosphere CO₂ fluxes, respectively, which were obtained from the optimized results of CarbonTracker 2011 (Peters, 2007); F_{ff} was fossil fuel emissions, adopted from the Regional Emission inventory in ASia (REAS, 2005 Asia monthly mean emission inventory) with a spatial resolution of 0.5° × 0.5° (Ohara et al., 2007); F_{fire} was biomass–burning emissions, provided by the monthly mean inventory at a spatial resolution of 0.5° × 0.5° from the Global Fire Emissions Database, Version 3 (GFED v3) (Van der Werf et al., 2010).

Firstly, the prior flux $F^0(x, y, z, t)$ was assumed as the true surface CO₂ flux. Forced by $F^0(x, y, z, t)$, the RAMS-CMAQ model was run to produce the artificial true CO₂ concentration results $C^0(x, y, z, t)$. Then, the artificial GOSAT observations y_t^{obs} (or $X_{\text{CO}_2}^0$) were generated using the observation operator in Eq. (7).

Secondly, the background surface CO₂ fluxes series $F^b(x, y, z, t)$ was created by

$$F^b(x, y, z, t) = (1.8 + \delta(x, y, z, t))F^0(x, y, z, t), \quad (22)$$

where δ was a random number. Driven by $F^b(x, y, z, t)$, the RAMS-CMAQ model was integrated to obtain the background CO₂ simulations $C^b(x, y, z, t)$. Then, the column-averaged concentrations $X_{\text{CO}_2}^b$ were obtained using Eq. (7).

A regional carbon flux data assimilation system

Z. Peng et al.

The performance of CFI-CMAQ was evaluated through a group of well-designed OSSEs. In all the OSSEs, the default ensemble size N was 48, the standard localization Schur radius c was 1280 km (20 grid spacing), and the covariance inflation factor of concentrations α was 1.1. The referenced lag-window was 9 days and the covariance inflation factor of scaling factors β was 70. Since the lag-window is very important for CO_2 transportation and β is a newly introduced parameter, both these parameters were further investigated by several numerical sensitivity experiments. The primary focus of this paper is to describe the assimilation methodology, so all the numerical experiments started on 1 January and ended on 30 March.

3.2 Experimental results

Essentially, CFI-CMAQ includes two parts: one for the CO_2 concentration assimilation with EnKF, which can provide a convincing CO_2 initial analysis field for the next assimilation cycle; and the other for the CO_2 flux optimization with EnKS. The EnKF part for the CO_2 concentration assimilation is independent of the EnKS part for the CO_2 flux inversion, but the performance of the EnKS part will be greatly influenced by the validation of the EnKF part.

We begin by describing the impacts of assimilating artificial observations $X_{\text{CO}_2}^0$ on CO_2 simulations. As shown in Fig. 4a, b and d, the monthly mean values of the background CO_2 concentrations C^b produced by the magnified surface CO_2 fluxes F^b were much larger than those of the artificial true CO_2 concentrations C^0 produced by the prior surface CO_2 fluxes F^0 near the surface in February 2010. In the east and south of China especially, the magnitude of the difference between C^0 and C^b was at least 6 ppmv. Also, as expected, the monthly mean $X_{\text{CO}_2}^b$ was much larger than the monthly mean artificial observations $X_{\text{CO}_2}^0$, and the magnitude of the difference between $X_{\text{CO}_2}^0$ and $X_{\text{CO}_2}^b$ reached 2 ppmv in the east and south of China (see Fig. 3b, c and e). However, the impact of magnifying surface CO_2 fluxes on the CO_2 concentrations was

[Title Page](#)[Abstract](#)[Introduction](#)[Conclusions](#)[References](#)[Tables](#)[Figures](#)[Back](#)[Close](#)[Full Screen / Esc](#)[Printer-friendly Version](#)[Interactive Discussion](#)

A regional carbon flux data assimilation system

Z. Peng et al.

Title Page

Abstract

Introduction

Conclusions

References

Tables

Figures



Back

Close

Full Screen / Esc

Printer-friendly Version

Interactive Discussion



primarily below the model-level 10 (approximately 6 km), and especially below level 7 (approximately 1.6 km). And above model level 10, the differences between C^0 and C^b fell to zero. After assimilating $X_{CO_2}^0$, the analysis CO_2 field C^a was much closer to C^0 (see Fig. 4c, e and f). The monthly mean difference between C^0 and C^a ranged from -2 to 2 ppmv and the relative error $(C^0 - C^a)/C^0$ ranged from -1 to 1% in almost the entire model domain at model-level 1. The monthly mean differences between C^0 and C^a were negligible above model-level 1. The monthly mean $X_{CO_2}^a$ was also closer to $X_{CO_2}^0$ and the difference between $X_{CO_2}^0$ and $X_{CO_2}^a$ ranged from -0.5 to 0.5 ppmv. In order to evaluate the general impact of assimilating $X_{CO_2}^0$ in the surface layer, time series of the daily mean CO_2 concentration extracted from the background simulations and the assimilations were compared with the artificial true simulations at four national background stations in China and their nearest large cities. As shown in Fig. 3a, Waliguan is 150 km away from Xining, Longfengshan is 180 km away from Haerbin, Shangdianzi is 150 km away from Beijing, and Linan is 50 km away from Hangzhou. The assimilated results are shown in Fig. 7. The background time series were much larger than the artificial true time series, especially at Shangdianzi, Beijing, Linan and Hangzhou, which are strongly influenced by local anthropogenic CO_2 emissions. After assimilating $X_{CO_2}^0$, the assimilated time series were very near to the true time series with negligible bias, as expected, at Waliguan, Xining, Shangdianzi, Beijing, Linan and Hangzhou, especially after the first 10 days, which can be considered the spin-up period. Meanwhile, the improvements at Longfengshan and Haerbin were limited due to the absence of observation data at those locations (see Fig. 3a). Nevertheless, in general, the substantial benefits to the CO_2 concentrations in the surface layer of assimilating GOSAT X_{CO_2} with EnKF are clear. All the results illustrated that EnKF can provide a convincing CO_2 initial analysis field for CO_2 flux inversion.

The impacts of assimilating $X_{CO_2}^0$ on surface CO_2 fluxes were also highly impressive. On the whole, the background surface CO_2 fluxes F^b were much larger than the prior true surface CO_2 fluxes F^0 in February 2010, especially in the east and south of

China. The monthly mean difference between F^b and F^0 reached $0.5 \mu\text{mole m}^{-2} \text{s}^{-1}$ in Jing-Jin-Ji, the Yangtze River Delta, and Pearl River Delta Urban Circle because of the strong local anthropogenic CO_2 emissions (see Fig. 7a, b and d). After assimilating $X_{\text{CO}_2}^0$, the assimilated surface CO_2 fluxes F^a decreased sharply. Thus, the monthly mean values of F^a were much smaller than F^b in most of the model domain in February 2010. The pattern of the difference between F^a and F^b was similar to that of the difference between F^0 and F^b (see Fig. 7b–e). The assimilated surface CO_2 fluxes were also compared to the artificial true fluxes F^0 , revealing that F^a was equivalent to F^0 in most of the model domain. The monthly mean difference between F^a and F^0 ranged from -0.01 to $0.01 \mu\text{mole m}^{-2} \text{s}^{-1}$ only (see Fig. 7f). In addition, the root-mean-square errors (RMSEs) of the assimilated flux members were analyzed. As shown in Fig. 8, the monthly mean RMSE was less than $0.05 \mu\text{mole m}^{-2} \text{s}^{-1}$ in most of the model domain, except in areas near to large cities such as Beijing, Shanghai and Guangzhou, indicating that the assimilated CO_2 fluxes were reliable.

In order to evaluate the ability of CFI-CMAQ to optimize the surface CO_2 fluxes comprehensively, the ratios of the monthly mean F^0 to the monthly mean F^b , which was similar to the monthly mean λ_t^b (where $\lambda_t^b = \sum_{i=1}^N \lambda_{i,t}^b / N$), but not the same, were analyzed. In actual implementation, we only analyzed the ratios where the absolute values of the monthly mean F^b were larger than 0.01, to avoid random noise. As shown in Fig. 9a, the ratios of the monthly mean F^0 to the monthly mean F^b ranged from 0.5 to 0.65 in most of China, except in the Qinghai–Tibet Plateau, where the absolute values of the monthly mean F^b were very small in February. The ratios varied greatly in the Indo-China Peninsula because of strong diurnal variation of CO_2 fluxes. In addition, the ratios of the monthly mean F^a to the monthly mean F^b and the ratios of the monthly mean F^a to the monthly mean F^0 are shown in Fig. 9b and c, respectively. These two figures demonstrate that the impact of the assimilation of $X_{\text{CO}_2}^0$ by CFI-CMAQ on

A regional carbon flux data assimilation system

Z. Peng et al.

Title Page

Abstract

Introduction

Conclusions

References

Tables

Figures



Back

Close

Full Screen / Esc

Printer-friendly Version

Interactive Discussion



CO₂ fluxes was great in the east and south of China in general, but the influence was negligible in Northeast China due to the lack of observation data.

In addition, time series of daily mean surface CO₂ fluxes extracted from F^b and F^a were compared with that from F^0 at four national background stations in China and their nearest large cities, similar to the CO₂ concentration assimilation. The results are shown in Fig. 9. The background time series were much larger than the artificial true time series, especially at Haerbin, Shangdianzi, Beijing, Linan and Hangzhou, which are strongly influenced by local anthropogenic CO₂ emissions. After assimilating $X_{CO_2}^0$, the assimilated time series were near to the true time series with acceptable bias, as expected, at Waliguan, Xining, Shangdianzi, Linan and Hangzhou after the 10 day spin-up period. However, the improvements at Longfengshan and Haerbin were negligible because of a lack of observations at these locations. Also, this inversion system failed to show improvements at Beijing because of an excessive impact of assimilation. Since the impact of assimilation $X_{CO_2}^0$ by CFI-CMAQ on CO₂ fluxes was in general greater in the east and south of China than other model areas (see Figs. 7e and 9b), the time series of the daily mean CO₂ fluxes in that area averaged from F^a was compared with those from F^b and F^0 , as well as their ratios (see Fig. 11). The two figures indicate that CFI-CMAQ could in general reproduce the true fluxes with acceptable bias.

A series of numerical experiments were conducted to investigate the sensitivity of the inflation factor of the scaling factors β and the lag-window. As shown in Fig. 11, CFI-CMAQ worked rather well for $\beta = 60, 70, 75, 80$. However, if β was much smaller than 50 (e.g. $\beta = 10$), the impact of assimilation was small due to the small ensemble spread; or if β was much larger than 80 (e.g. $\beta = 100$), the assimilated CO₂ fluxes deviated markedly from the “true” CO₂ fluxes. In other words, the performance of CFI-CMAQ greatly relies on the choice of β . From the perspective of the lag-window, the differences among the four assimilation sensitivity experiments with lag-windows of 3, 6, 9 and 12 days were very small (see Fig. 12). Although Peters et al. (2007) indicated that the lag-window should be more than five weeks, it seems that the smoother window had a slight influence on the assimilated results for CFI-CMAQ. It is clear that the

A regional carbon flux data assimilation system

Z. Peng et al.

Title Page

Abstract

Introduction

Conclusions

References

Tables

Figures



Back

Close

Full Screen / Esc

Printer-friendly Version

Interactive Discussion



assimilated results with a larger lag-window were better than those with a smaller lag-window; however, CFI-CMAQ performed very well even with a short lag-window (e.g. 3 days).

4 Summary and conclusions

A regional surface CO₂ flux inversion system, CFI-CMAQ, has been developed to optimize CO₂ fluxes at finer scales. It operates under a joint data assimilation framework, simultaneously assimilating CO₂ concentrations and surface CO₂ fluxes, similar to Kang et al. (2011, 2012) and Tian et al. (2013). The smoothing operator, which was first adopted by Peters et al. (2005) as the persistence dynamical model, is associated with the atmospheric transport model for the purpose of resolving the “signal-to-noise” problem, as well as transporting the useful observed information onto the next assimilation cycle, in order to optimize the surface CO₂ fluxes as a whole at the grid scale. In this application, the scaling factors to be optimized in the flux inversion system can be forecast at the grid scale without random noise. The OSSEs showed that the performance of CFI-CMAQ is effective and promising. In general, it could reproduce the true fluxes at finer scales with acceptable bias.

This study represents the first step in developing a regional surface CO₂ flux inversion system to optimize CO₂ fluxes over East Asia, particularly over China. In future, we intend to further develop the covariance localization techniques and inflation techniques to improve the performance of CFI-CMAQ. Furthermore, the uncertainty of the boundary conditions should be considered to improve the effectiveness of regional CO₂ flux optimization.

Acknowledgements. This work was supported by the Strategic Priority Research Program—Climate Change: Carbon Budget and Relevant Issues (XDA05040404), the National High Technology Research and Development Program of China (2013AA122002). CarbonTracker results used to generate the initial condition are provided by NOAA ESRL, Boulder, Colorado, USA from the website at <http://carbontracker.noaa.gov>. The numerical calculations in this paper

A regional carbon flux data assimilation system

Z. Peng et al.

Title Page

Abstract

Introduction

Conclusions

References

Tables

Figures



Back

Close

Full Screen / Esc

Printer-friendly Version

Interactive Discussion



have been done on the IBM Blade cluster system in the High Performance Computing Center (HPCC) of Nanjing University.

References

- Andres, R. J., Boden, T. A., Bréon, F.-M., Ciais, P., Davis, S., Erickson, D., Gregg, J. S., Jacobson, A., Marland, G., Miller, J., Oda, T., Olivier, J. G. J., Raupach, M. R., Rayner, P., and Treanton, K.: A synthesis of carbon dioxide emissions from fossil-fuel combustion, *Biogeosciences*, 9, 1845–1871, doi:10.5194/bg-9-1845-2012, 2012.
- Baker, D. F., Doney, S. C., and Schimel, D. S.: Variational data assimilation for atmospheric CO₂, *Tellus B*, 58, 359–365, 2006.
- Boden, T. A., Marland, G., and Andres, R. J.: Global, Regional, and National Fossil-Fuel CO₂ Emissions. Carbon Dioxide Information Analysis Center, Oak Ridge National Laboratory, US Department of Energy, Oak Ridge, TN, USA, doi:10.3334/CDIAC/00001_V2011, 2011.
- Chevallier, F.: Impact of correlated observation errors on inverted CO₂ surface fluxes from OCO measurements, *Geophys. Res. Lett.*, 34, L24804, doi:10.1029/2007GL030463, 2007.
- Chevallier, F. M. F., Peylin, P., Bousquet, S. S. P., Bréon, F.-M., Chédin, A., and Ciais, P.: Inferring CO₂ sources and sinks from satellite observations: Method and application to TOVS data, *J. Geophys. Res.*, 110, D24309, doi:10.1029/2005JD006390, 2005.
- Chevallier, F., Bréon, F.-M., and Rayner, P. J.: Contribution of the Orbiting Carbon Observatory to the estimation of CO₂ sources and sinks: theoretical study in a variational data assimilation framework, *J. Geophys. Res.*, 112, D09307, doi:10.1029/2006JD007375, 2007.
- Connor, B. J., Bösch, H., Toon, G., Sen, B., Miller, C., and Crisp, D.: Orbiting carbon observatory: inverse method and prospective error analysis, *J. Geophys. Res.*, 113, D05305, doi:10.1029/2006JD008336, 2008.
- Crisp, D., Bösch, H., Brown, L., Castano, R., Christi, M., Connor, B., Frankenberg, C., McDuffie, J., Miller, C. E., Natraj, V., O'Dell, C., O'Brien, D., Polonsky, I., Oyafuso, F., Thompson, D., Toon, G., and Spurr, R.: OCO (Orbiting Carbon Observatory)-2 Level 2 Full Physics Retrieval Algorithm Theoretical Basis, Tech. Rep. OCO D-65488, NASA Jet Propulsion Laboratory, California Institute of Technology, Pasadena, CA, version 1.0 Rev 4, available at: http://disc.sci.gsfc.nasa.gov/acdisc/documentation/OCO-2_L2_FP_ATBD_v1_rev4_Nov10.pdf, last access: 4 August 2014), 2010.

A regional carbon flux data assimilation system

Z. Peng et al.

Title Page

Abstract

Introduction

Conclusions

References

Tables

Figures



Back

Close

Full Screen / Esc

Printer-friendly Version

Interactive Discussion



A regional carbon flux data assimilation system

Z. Peng et al.

Title Page

Abstract

Introduction

Conclusions

References

Tables

Figures



Back

Close

Full Screen / Esc

Printer-friendly Version

Interactive Discussion



- Crisp, D., Fisher, B. M., O'Dell, C., Frankenberg, C., Basilio, R., Bösch, H., Brown, L. R., Castano, R., Connor, B., Deutscher, N. M., Eldering, A., Griffith, D., Gunson, M., Kuze, A., Mandrake, L., McDuffie, J., Messerschmidt, J., Miller, C. E., Morino, I., Natraj, V., Notholt, J., O'Brien, D. M., Oyafuso, F., Polonsky, I., Robinson, J., Salawitch, R., Sherlock, V., Smyth, M., Suto, H., Taylor, T. E., Thompson, D. R., Wennberg, P. O., Wunch, D., and Yung, Y. L.: The ACOS CO₂ retrieval algorithm – Part II: Global X_{CO₂} data characterization, *Atmos. Meas. Tech.*, 5, 687–707, doi:10.5194/amt-5-687-2012, 2012.
- Deng, F., Chen, J. M., Ishizawa, M., YUEN, C. W. A. I., Mo, G., Higuchi, K., Chan, D., and Maksyutov, S.: Global monthly CO₂ flux inversion with a focus over North America, *Tellus B*, 59, 179–190, 2007.
- Engelen, R. J., Serrar, S., and Chevallier, F.: Four-dimensional data assimilation of atmospheric CO₂ using AIRS observations, *J. Geophys. Res.*, 114, D03303, doi:10.1029/2008JD010739, 2009.
- Feng, L., Palmer, P. I., Bösch, H., and Dance, S.: Estimating surface CO₂ fluxes from space-borne CO₂ dry air mole fraction observations using an ensemble Kalman Filter, *Atmos. Chem. Phys.*, 9, 2619–2633, doi:10.5194/acp-9-2619-2009, 2009.
- Feng, L., Palmer, P. I., Yang, Y., Yantosca, R. M., Kawa, S. R., Paris, J.-D., Matsueda, H., and Machida, T.: Evaluating a 3-D transport model of atmospheric CO₂ using ground-based, aircraft, and space-borne data, *Atmos. Chem. Phys.*, 11, 2789–2803, doi:10.5194/acp-11-2789-2011, 2011.
- Gurney, K. R., Law, R. L., Denning, A. S., Rayner, P. J., Baker, D., Bousquet, P., Bruhwiler, L., Chen, Y. H., Ciais, P., Fan, S., Fung, I. Y., Gloor, M., Heimann, M., Higuchi, K., John, J., Maki, T., Maksyutov, S., Masarie, K., Peylin, P., Prather, M., Pak, B. C., Randerson, J., Sarmiento, J., Taguchi, S., Takahashi, T., and Yuen, C. W.: Towards robust regional estimates of CO₂ sources and sinks using atmospheric transport models, *Nature*, 415, 626–630, 2002.
- Gurney, K. R., Mendoza, D. L., Zhou, Y. Y., Fischer, M. L., Miller, C. C., Geethakumar, S. and Du Can, S. D.: High resolution fossil fuel combustion CO₂ emission fluxes for the United States, *Environ. Sci. Technol.*, 43, 5535–5541, doi:10.1021/es900806c, 2009.
- Houtekamer, P. L. and Mitchell, H. L.: A sequential ensemble Kalman filter for atmospheric data assimilation, *Mon. Weather Rev.*, 129, 123–137, 2001.
- Huang, Z. K., Peng, Z., Liu, H. N., and Zhang, M. G.: Development of CMAQ for East Asia CO₂ data assimilation under an EnKF framework: a first result, *Chinese Sci. Bull.*, 59, 3200–3208, doi:10.1007/s11434-014-0348-9, 2014.

A regional carbon flux data assimilation system

Z. Peng et al.

Title Page

Abstract

Introduction

Conclusions

References

Tables

Figures



Back

Close

Full Screen / Esc

Printer-friendly Version

Interactive Discussion



IPCC: Climate Change 2007: Synthesis Report. Contribution of Working Groups I, II and III to the Fourth Assessment Report of the Intergovernmental Panel on Climate Change, Core Writing Team, edited by: Pachauri, R. K. and Reisinger, A., IPCC, Cambridge University Press, Cambridge, 2007.

5 IPCC AR5 WG1: Climate Change 2013: The Physical Science Basis. Working Group 1 (WG1) Contribution to the Intergovernmental Panel on Climate Change (IPCC) 5th Assessment Report (AR5), edited by: Stocker, T. F., Qin D., Plattner, G., Tignor, M. M. B., Allen, S., Boschung, J., Nauels, A., Xia, Y., Bex, V., and Midgley, P., Climate Change 2013 Working Group 1 website, Cambridge University Press, Cambridge, United Kingdom and New York, NY, USA, 2013.

10 Jiang, F., Wang, H. W., Chen, J. M., Zhou, L. X., Ju, W. M., Ding, A. J., Liu, L. X., and Peters, W.: Nested atmospheric inversion for the terrestrial carbon sources and sinks in China, Biogeosciences, 10, 5311–5324, doi:10.5194/bg-10-5311-2013, 2013.

15 Kang, J.-S., Kalnay, E., Liu, J., Fung, I., Miyoshi, T., and Ide, K.: “Variable localization” in an ensemble Kalman filter: application to the carbon cycle data assimilation, J. Geophys. Res., 116, D09110, doi:10.1029/2010JD014673, 2011.

Kang, J.-S., Kalnay, E., Miyoshi, T., Liu, J., and Fung, I.: Estimation of surface carbon fluxes with an advanced data assimilation methodology, J. Geophys. Res., 117, D24101, doi:10.1029/2012JD018259, 2012.

20 Kou, X., Zhang, M., and Peng, Z.: Numerical simulation of CO₂ concentrations in East Asia with RAMS-CMAQ, Atmos. Ocean. Sc. Lett., 6, 179–184, 2013.

Kretschmer, R., Gerbig, C., Karstens, U., and Koch, F.-T.: Error characterization of CO₂ vertical mixing in the atmospheric transport model WRF-VPRM, Atmos. Chem. Phys., 12, 2441–2458, doi:10.5194/acp-12-2441-2012, 2012.

25 Liu, J., Fung, I., Kalnay, E., and Kang, J.: CO₂ transport uncertainties from the uncertainties in meteorological fields, Geophys. Res. Lett., 38, L12808, doi:10.1029/2011GL047213, 2011.

Liu, J., Fung, I., Kalnay, E., Kang, J.-S., Olsen, E. T., and Chen, L.: Simultaneous assimilation of AIRS X_{CO₂} and meteorological observations in a carbon climate model with an ensemble Kalman filter, J. Geophys. Res., 117, D05309, doi:10.1029/2011JD016642, 2012.

30 Liu Z., Bambha, R. P., and Pinto, J. P.: Toward verifying fossil fuel CO₂ emissions with the Community Multi-scale Air Quality (CMAQ) model: motivation, model description and initial simulation, J. Air Waste Manage., 64, 419–435, doi:10.1080/10962247.2013.816642, 2013.

A regional carbon flux data assimilation system

Z. Peng et al.

Title Page

Abstract

Introduction

Conclusions

References

Tables

Figures



Back

Close

Full Screen / Esc

Printer-friendly Version

Interactive Discussion



- Marland, G.: Uncertainties in accounting for CO₂ from fossil fuels, *J. Ind. Ecol.*, 12, 136–139, doi:10.1111/j.1530-9290.2008.00014.x, 2008.
- Miyazaki K.: Performance of a local ensemble transform Kalman filter for the analysis of atmospheric circulation and distribution of long-lived tracers under idealized conditions, *J. Geophys. Res.*, 114, D19304, doi:10.1029/2009JD011892, 2009.
- O'Dell, C. W., Connor, B., Bösch, H., O'Brien, D., Frankenberg, C., Castano, R., Christi, M., Eldering, D., Fisher, B., Gunson, M., McDuffie, J., Miller, C. E., Natraj, V., Oyafuso, F., Polonsky, I., Smyth, M., Taylor, T., Toon, G. C., Wennberg, P. O., and Wunch, D.: The ACOS CO₂ retrieval algorithm – Part 1: Description and validation against synthetic observations, *Atmos. Meas. Tech.*, 5, 99–121, doi:10.5194/amt-5-99-2012, 2012.
- Peters, W., Miller, J. B., Whitaker, J., Denning, A. S., Hirsch, A., Krol, M. C., Zupanski, D., Bruhwiler, L., and Tans, P. P.: An ensemble data assimilation system to estimate CO₂ surface fluxes from atmospheric trace gas observations, *J. Geophys. Res.*, 110, D24304, doi:10.1029/2005JD006157, 2005.
- Peters, W., Jacobson, A. R., Sweeney, C., Andrews, A. E., Conway, T. J., Masarie, K., Miller, J. B., Bruhwiler, L. M. P., Petron, G., Hirsch, A. I., Worthy, D. E. J., van der Werf, G. R., Randerson, J. T., Wennberg, P. O., Krol, M. C., and Tans, P. P.: An atmospheric perspective on North American carbon dioxide exchange: CarbonTracker, *P. Natl. Acad. Sci. USA*, 104, 18925–18930, 2007.
- Peters, W., Krol, M. C., Van Der Werf, G. R., Houwling, S., Jones, C. D., Hughes, J., Schaefer, K., Masarie, K. A., Jacobson, A. R., Miller, J. B., Cho, C. H., Ramonet, M., Schmidt, M., Ciattaglia, L., Apadula, F., Heltai, D., Meinhardt, F., Di Sarra, A. G., Piachentina, S., Sferlazzo, D., Aalto, T., Hatakka, J., Ström, J., Haszpra, L., Meijer, H. A. J., Van Der Laan, S., Neubert, R. E. M., Jordan, A., Rodo, X., Morgui, J.-A., Vermeulen, A. T., Popa, E., Rozanski, M., Manning, A. C., Leuenberger, M., Uglietti, C., Dolman, A. J., Ciais, P., Heimann, M., and Tans, P. P.: Seven years of recent European net terrestrial carbon dioxide exchange constrained by atmospheric observations, *Global Change Biol.*, 16, 1365–2486, 2009.
- Peylin, P., Law, R. M., Gurney, K. R., Chevallier, F., Jacobson, A. R., Maki, T., Niwa, Y., Patra, P. K., Peters, W., Rayner, P. J., Rödenbeck, C., van der Laan-Luijkx, I. T., and Zhang, X.: Global atmospheric carbon budget: results from an ensemble of atmospheric CO₂ inversions, *Biogeosciences*, 10, 6699–6720, doi:10.5194/bg-10-6699-2013, 2013.
- Pillai, D., Gerbig, C., Ahmadov, R., Rödenbeck, C., Kretschmer, R., Koch, T., Thompson, R., Neininger, B., and Lavrié, J. V.: High-resolution simulations of atmospheric CO₂ over complex

**A regional carbon
flux data assimilation
system**

Z. Peng et al.

[Title Page](#)[Abstract](#)[Introduction](#)[Conclusions](#)[References](#)[Tables](#)[Figures](#)[Back](#)[Close](#)[Full Screen / Esc](#)[Printer-friendly Version](#)[Interactive Discussion](#)

terrain – representing the Ochsenkopf mountain tall tower, *Atmos. Chem. Phys.*, 11, 7445–7464, doi:10.5194/acp-11-7445-2011, 2011.

Prather, M., Zhu, X., Strahan, S. E., Steenrod, S., D., and Rodriguez, J., M.: Quantifying errors in trace species transport modeling, *P. Natl. Acad. Sci. USA*, 105, 19617–19621, doi:10.1073/pnas.0806541106, 2008.

National Research Council: *Verifying Greenhouse Gas Emissions: Methods to Support International Climate Agreements*, The National Academies Press, Washington, D.C., 2010.

Tian, X., Xie, Z., and Sun, Q.: A POD-based ensemble four-dimensional variational assimilation method, *Tellus A*, 63, 805–816, 2011.

Tian, X., Xie, Z., Liu, Y., Cai, Z., Fu, Y., Zhang, H., and Feng, L.: A joint data assimilation system (Tan-Tracker) to simultaneously estimate surface CO₂ fluxes and 3-D atmospheric CO₂ concentrations from observations, *Atmos. Chem. Phys. Discuss.*, 13, 24755–24784, doi:10.5194/acpd-13-24755-2013, 2013.

van der Werf, G. R., Randerson, J. T., Giglio, L., Collatz, G. J., Mu, M., Kasibhatla, P. S., Morton, D. C., DeFries, R. S., Jin, Y., and van Leeuwen, T. T.: Global fire emissions and the contribution of deforestation, savanna, forest, agricultural, and peat fires (1997–2009), *Atmos. Chem. Phys.*, 10, 11707–11735, doi:10.5194/acp-10-11707-2010, 2010.

Wang, B., Liu, J., Wang, S., Cheng, W., Liu, J., Liu, C., Xiao Q., and Kuo, Y.: An economical approach to four-dimensional variational data assimilation, *Adv. Atmos. Sci.*, 27, 715–727, doi:10.1007/s00376-009-9122-3, 2010.

Zhang, H. F., Chen, B. Z., van der Laan-Luijkx, I. T., Chen, J., Xu, G., Yan, J. W., Zhou, L. X., Fukuyama, Y., Tans, P. P., and Peters, W.: Net terrestrial CO₂ exchange over China during 2001–2010 estimated with an ensemble data assimilation system for atmospheric CO₂, *J. Geophys. Res. Atmos.*, 119, 3500–3515, doi:10.1002/2013JD021297, 2014a.

Zhang, H. F., Chen, B. Z., Machida, T., Matsueda, H., Sawa, Y., Fukuyama, Y., Langenfelds, R., van der Schoot, M., Xu, G., Yan, J. W., Cheng, M. L., Zhou, L. X., Tans, P. P., and Peters, W.: Estimating Asian terrestrial carbon fluxes from CONTRAIL aircraft and surface CO₂ observations for the period 2006–2010, *Atmos. Chem. Phys.*, 14, 5807–5824, doi:10.5194/acp-14-5807-2014, 2014b.

Zhang, M., Uno, I., Sugata, S., Wang, Z., Byun, D., and Akimoto, H.: Numerical study of boundary layer ozone transport and photochemical production in East Asia in the wintertime, *Geophys. Res. Lett.*, 29, 40-1–40-4, doi:10.1029/2001GL014368, 2002.

Zhang, M., Uno, I., Carmichael, G. R., Akimoto, H., Wang, Z., Tang, Y., Woo, J., Streets, D. G., Sachse, G. W., Avery, M. A., Weber, R. J., and Talbot, R. W.: Large-scale structure of trace gas and aerosol distributions over the western Pacific Ocean during the Transport and Chemical Evolution Over the Pacific (TRACE-P) experiment, *J. Geophys. Res.*, 108, 8820, doi:10.1029/2002JD002946, 2003.

Zhang, M., Gao, L., Ge, C., and Xu, Y.: Simulation of nitrate aerosol concentrations over East Asia with the model system RAMS-CMAQ, *Tellus B*, 59, 372–380, 2007.

A regional carbon flux data assimilation system

Z. Peng et al.

Title Page

Abstract

Introduction

Conclusions

References

Tables

Figures



Back

Close

Full Screen / Esc

Printer-friendly Version

Interactive Discussion



A regional carbon flux data assimilation system

Z. Peng et al.

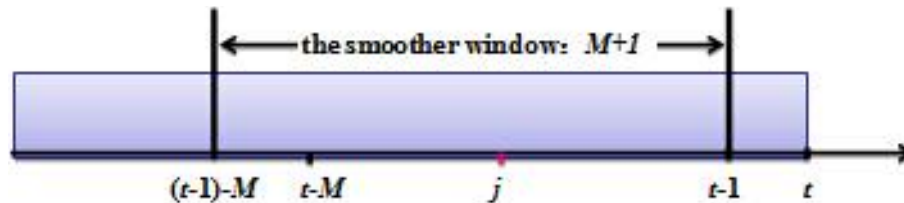


Figure 1. Schematic diagram of the smoother window.

[Title Page](#)[Abstract](#)[Introduction](#)[Conclusions](#)[References](#)[Tables](#)[Figures](#)[Back](#)[Close](#)[Full Screen / Esc](#)[Printer-friendly Version](#)[Interactive Discussion](#)

A regional carbon flux data assimilation system

Z. Peng et al.

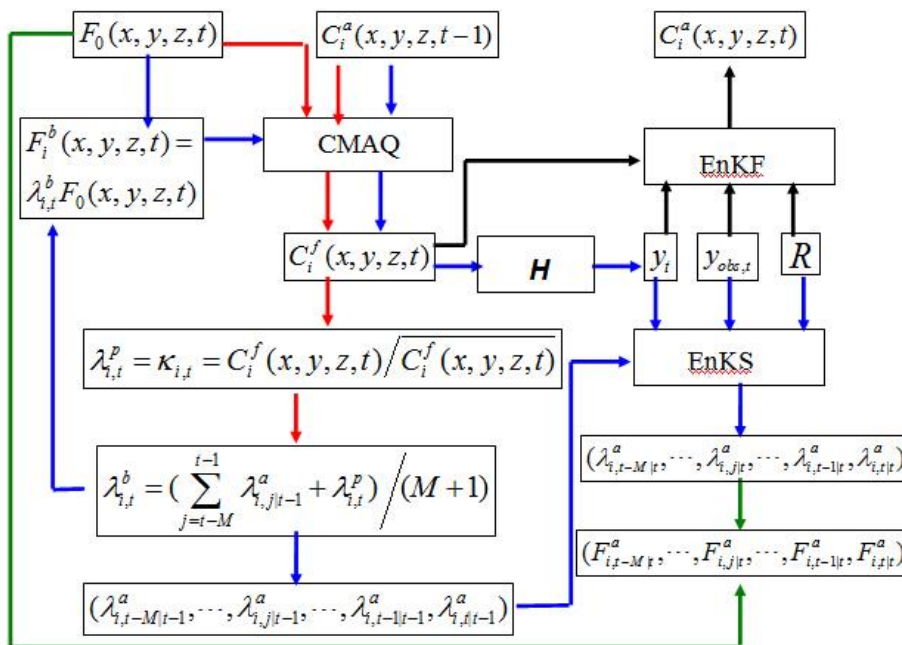


Figure 2. Flowchart of the CFI-CMAQ system used to optimize surface CO₂ fluxes. The system includes the following four parts at each optimization cycle: (1) forecasting of the background linear scaling factors $\lambda_{i,t}^b$ (red arrows); (2) optimization of the scaling factors in the smoother window M by EnKS (see Fig. 1) (blue arrows); (3) updating of the flux in the smoother window (green arrows); and (4) assimilation of the CO₂ concentration fields at time t by EnKF (black arrows).

Title Page	
Abstract	Introduction
Conclusions	References
Tables	Figures
◀	▶
◀	▶
Back	Close
Full Screen / Esc	
Printer-friendly Version	
Interactive Discussion	



A regional carbon flux data assimilation system

Z. Peng et al.

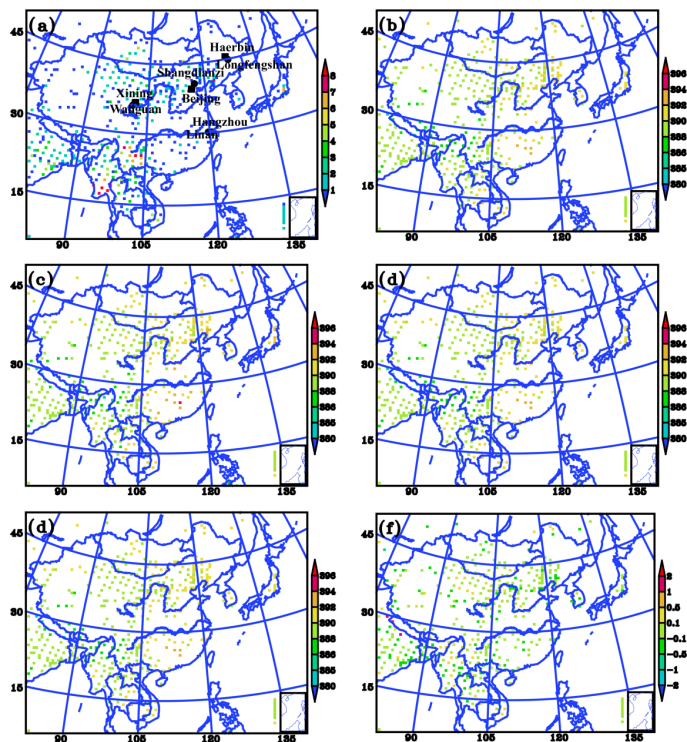


Figure 3. (a) Total number of observations in February 2010 in the model grid. Each symbol indicates the total number of all GOSAT X_{CO_2} measurements in the corresponding model grid. Monthly mean values of (b) $X_{\text{CO}_2}^0$, column mixing ratio of C^0 ; (c) $X_{\text{CO}_2}^b$, column mixing ratio of C^b ; (d) $X_{\text{CO}_2}^a$, column mixing ratio of C^a ; (e) $X_{\text{CO}_2}^0 - X_{\text{CO}_2}^b$; (f) $X_{\text{CO}_2}^0 - X_{\text{CO}_2}^a$; and (g) $X_{\text{CO}_2}^a - X_{\text{CO}_2}^b$. All column mixing ratios are column-averaged with real GOSAT X_{CO_2} averaging kernels at GOSAT X_{CO_2} locations. Each symbol indicates the monthly average value of all X_{CO_2} estimates in the model grid.

Title Page

Abstract

Introduction

Conclusions

References

Tables

Figures



Back

Close

Full Screen / Esc

Printer-friendly Version

Interactive Discussion



A regional carbon flux data assimilation system

Z. Peng et al.

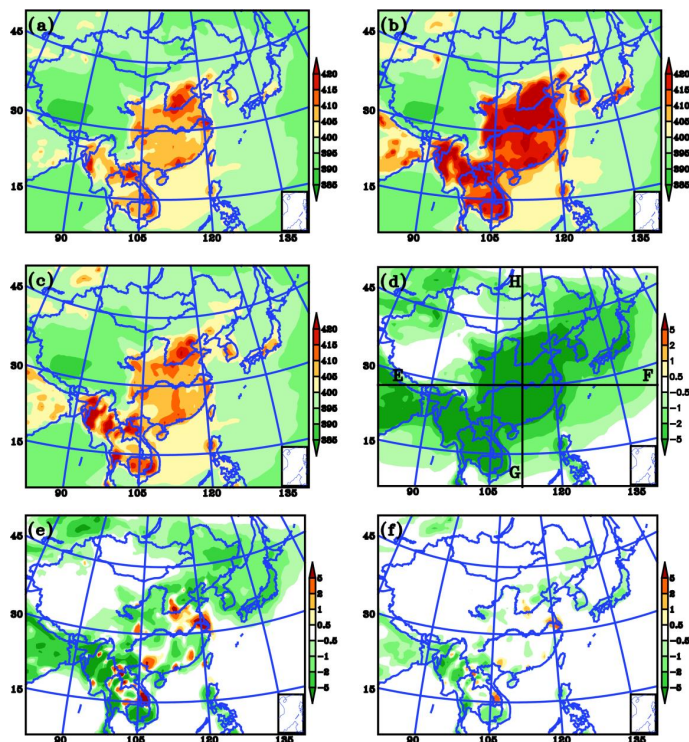


Figure 4. Monthly mean values of **(a)** C^0 , the artificial true simulations driven by the prior surface CO_2 fluxes F^0 ; **(b)** C^b , the background simulations driven by magnified surface CO_2 fluxes $F^b = 1.8 \cdot F^0$; **(c)** C^a , assimilations; **(d)** $C^0 - C^b$; **(e)** $C^0 - C^a$; and **(f)** $100 \cdot (C^0 - C^a) / C^0$ at model-level 1 in February 2010. Black lines EF and GH indicate the positions of the cross sections shown in Fig. 5.

[Title Page](#)
[Abstract](#)
[Introduction](#)
[Conclusions](#)
[References](#)
[Tables](#)
[Figures](#)
[◀](#)
[▶](#)
[◀](#)
[▶](#)
[Back](#)
[Close](#)
[Full Screen / Esc](#)
[Printer-friendly Version](#)
[Interactive Discussion](#)


A regional carbon flux data assimilation system

Z. Peng et al.

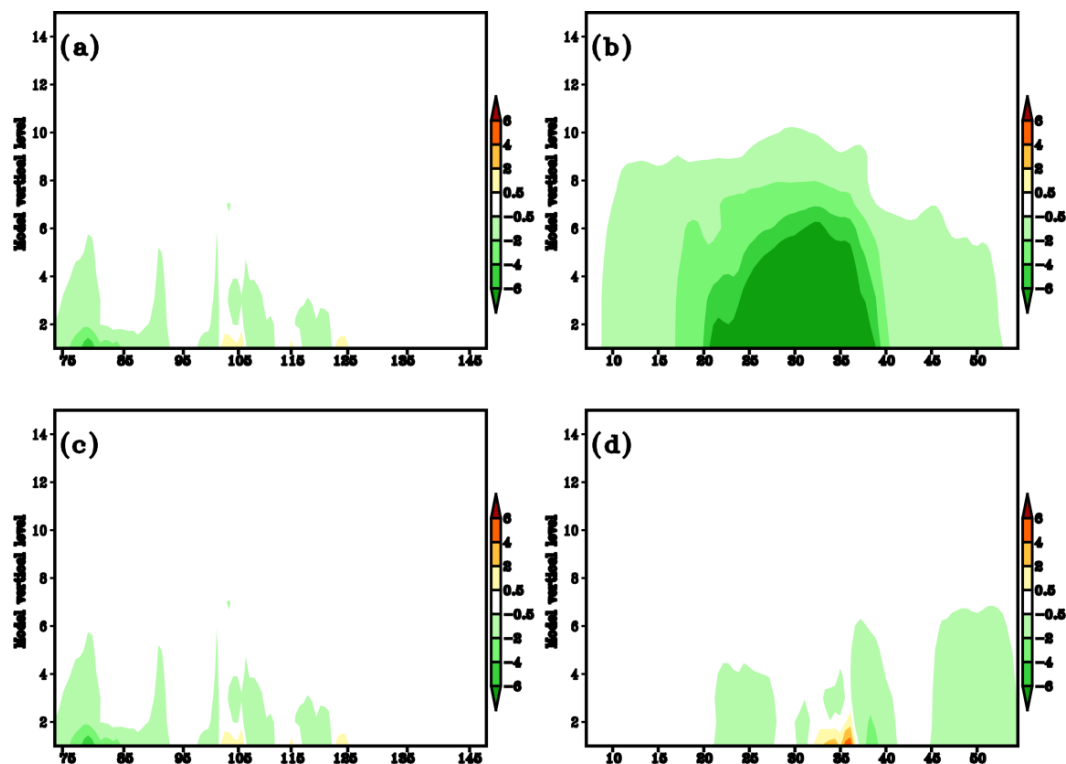


Figure 5. Monthly mean cross sections of $C^0 - C^b$ along line (a) EF and (b) GH, and monthly mean cross sections of $C^0 - C^a$ along line (c) EF and (d) GH (cross section lines shown in Fig. 4d).

A regional carbon flux data assimilation system

Z. Peng et al.

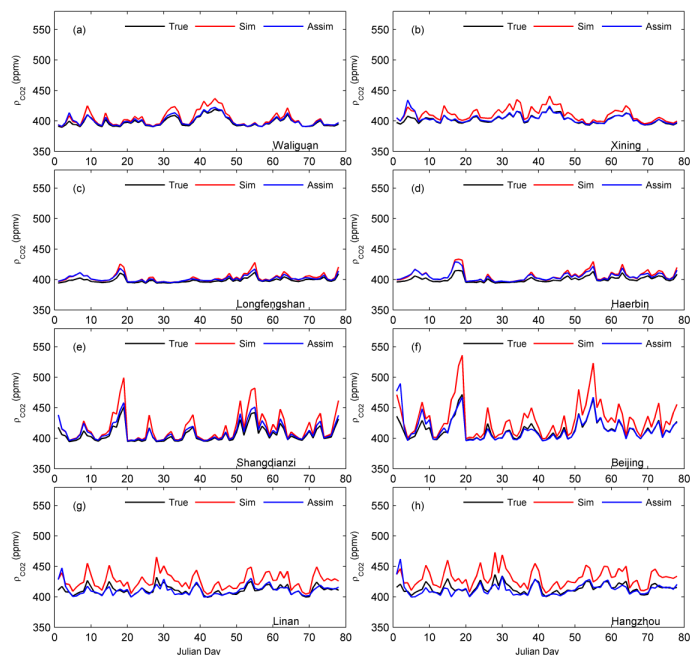


Figure 6. Daily mean time series of CO_2 concentrations at national background stations in China and their nearest large cities from 1 January to 20 March 2010 extracted from the artificial true simulations C^0 (black), background simulations C^b (red), and assimilations (blue). All time series were interpolated to the observation locations by the spatial bilinear interpolator method. The sites used are **(a)** Waliguan (36.28°N , 100.91°E), **(b)** Xining (36.56°N , 101.74°E), **(c)** Longfengshan (44.73°N , 127.6°E), **(d)** Haerbin (45.75°N , 126.63°E), **(e)** Shangdianzi (40.65°N , 117.12°E), **(f)** Beijing (39.92°N , 116.46°E), **(g)** Linan (30.3°N , 119.73°E), and **(h)** Hangzhou (30.3°N , 120.2°E).

[Title Page](#)
[Abstract](#)
[Introduction](#)
[Conclusions](#)
[References](#)
[Tables](#)
[Figures](#)
[◀](#)
[▶](#)
[◀](#)
[▶](#)
[Back](#)
[Close](#)
[Full Screen / Esc](#)
[Printer-friendly Version](#)
[Interactive Discussion](#)


A regional carbon flux data assimilation system

Z. Peng et al.

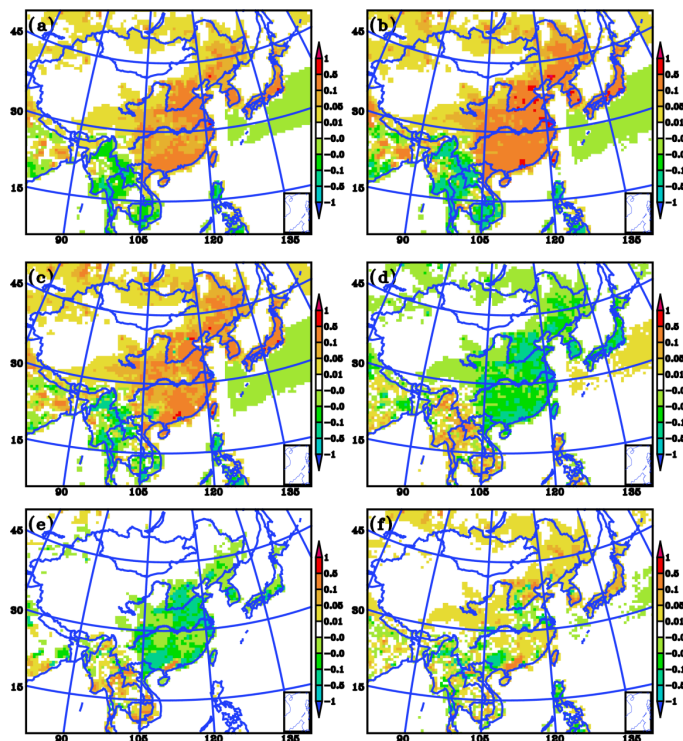


Figure 7. Monthly mean values in February 2010 of **(a)** F^0 , the prior true surface CO_2 fluxes; **(b)** F^b , the background CO_2 fluxes, $F^b(x, y, z, t) = (1.8 + \delta)F^0(x, y, z, t)$; **(c)** F^a , the assimilated surface CO_2 fluxes; **(d)** $F^0 - F^b$; **(e)** $F^a - F^b$; and **(f)** $F^a - F^0$ (units: $\mu\text{mole m}^{-2} \text{s}^{-1}$).

Title Page

Abstract

Introduction

Conclusions

References

Tables

Figures



Back

Close

Full Screen / Esc

Printer-friendly Version

Interactive Discussion



A regional carbon flux data assimilation system

Z. Peng et al.

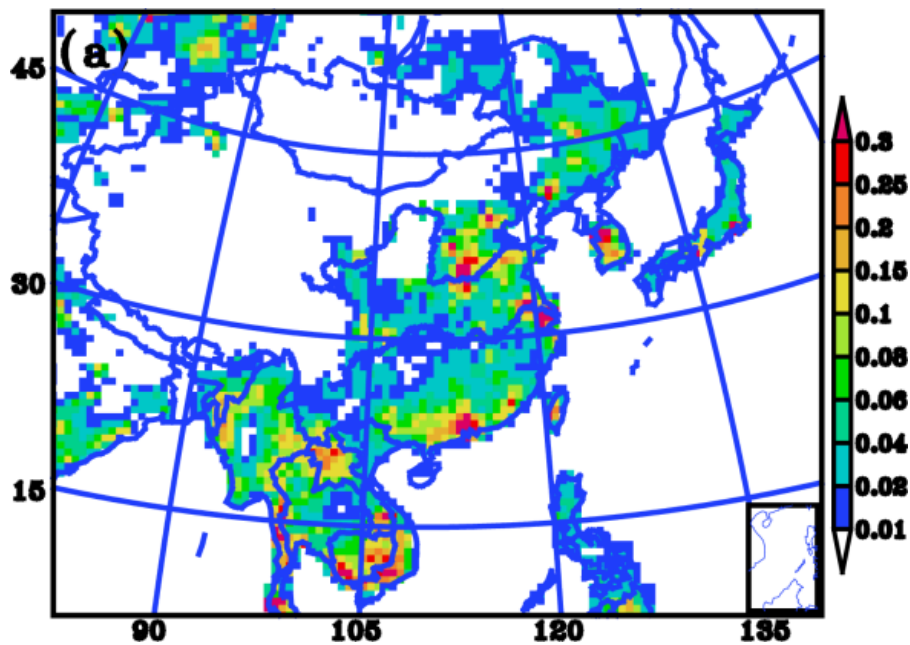


Figure 8. Monthly mean RMSEs of F^a in February 2010 (units: $\mu\text{mole m}^{-2} \text{s}^{-1}$).

[Title Page](#)[Abstract](#)[Introduction](#)[Conclusions](#)[References](#)[Tables](#)[Figures](#)[◀](#)[▶](#)[◀](#)[▶](#)[Back](#)[Close](#)[Full Screen / Esc](#)[Printer-friendly Version](#)[Interactive Discussion](#)

A regional carbon flux data assimilation system

Z. Peng et al.

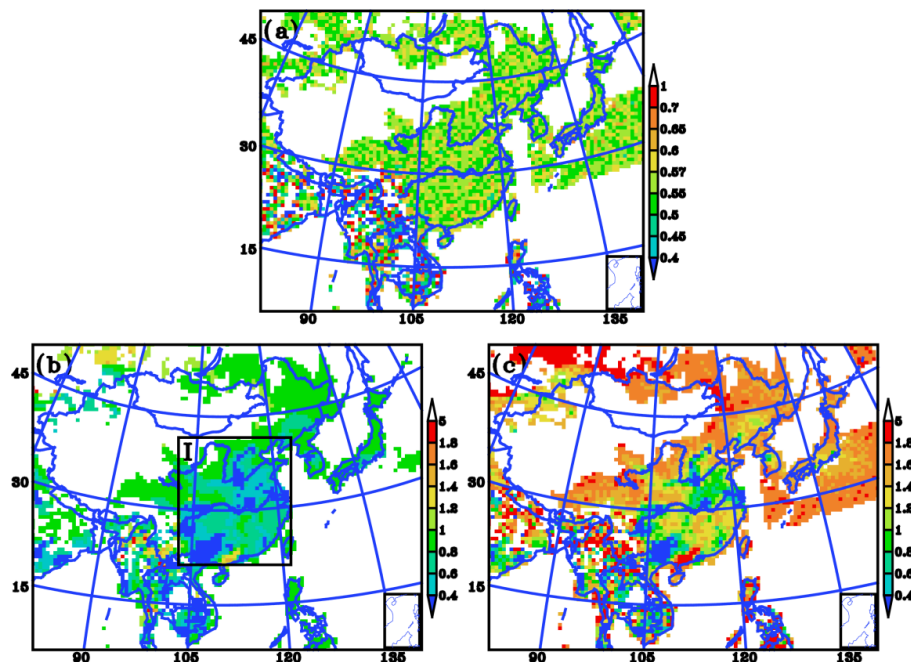


Figure 9. (a) Ratios of monthly mean F^0 to monthly mean F^b ; (b) ratios of monthly mean F^a to monthly mean F^b ; and (c) ratios of monthly mean F^a to monthly mean F^0 in February 2010. The white part indicates the ratios where the absolute values of monthly mean F^b are larger than 0.01, not analyzed in this study. The black square labeled I indicates the domain where surface CO_2 fluxes were used for the results presented in Fig. 12.

Title Page

Abstract

Introduction

Conclusions

References

Tables

Figures



Back

Close

Full Screen / Esc

Printer-friendly Version

Interactive Discussion



A regional carbon flux data assimilation system

Z. Peng et al.

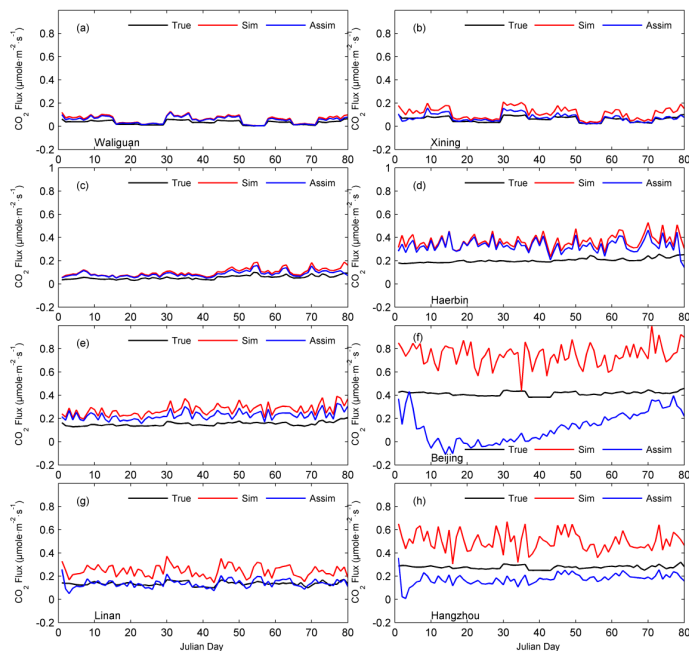


Figure 10. Daily mean time series of CO_2 fluxes at national background stations in China and their nearest large cities from 1 January to 20 March 2010 extracted from the prior true surface CO_2 fluxes F^0 (black), background CO_2 fluxes F^b (red), and assimilated CO_2 fluxes F^a (blue). All time series were interpolated to the observation locations by the spatial bilinear interpolator method. The sites used are (a) Waliguan, (b) Xining, (c) Longfengshan, (d) Haerbin, (e) Shangdianzi, (f) Beijing, (g) Linan, and (h) Hangzhou.

Title Page

Abstract

Introduction

Conclusions

References

Tables

Figures



Back

Close

Full Screen / Esc

Printer-friendly Version

Interactive Discussion



A regional carbon flux data assimilation system

Z. Peng et al.

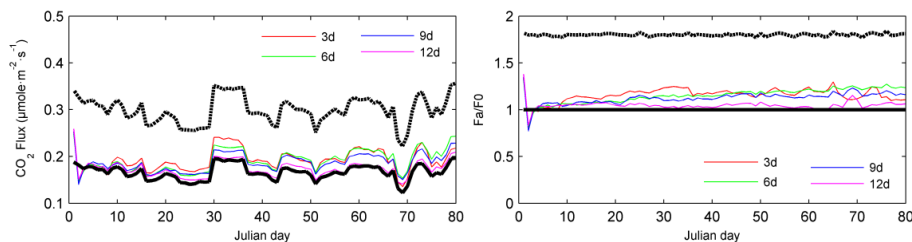


Figure 12. Time series of daily mean CO₂ fluxes averaged in domain I (shown in Fig. 9b) from 1 January to 20 March 2010 with different smoother windows (3, 6, 9 and 12 days). The black dashed line is the time series averaged from F^b and the black solid line is the time series averaged from F^0 .

[Title Page](#)[Abstract](#)[Introduction](#)[Conclusions](#)[References](#)[Tables](#)[Figures](#)[Back](#)[Close](#)[Full Screen / Esc](#)[Printer-friendly Version](#)[Interactive Discussion](#)